Journal of Thermal Analysis and Calorimetry (2018) 133:869–879
https://doi.org/10.1007/s10973-018-7152-8

CO_2 adsorption and desorption properties of calcined layered double hydroxides

Effect of metal composition on the LDH structure

S. Colonna[1] · M. Bastianini[2] · M. Sisani[2] · A. Fina[1]

Received: 31 October 2017 / Accepted: 1 March 2018 / Published online: 10 March 2018

Abstract
In this study, the CO_2 adsorption properties of different metal mixed oxides (MMO) obtained by calcination of different layered double hydroxides (LDH) are addressed. Four types of LDH, with composition $\left[M^{2+}_{1-X}M^{3+}_{x}(OH)_2\right]^{x+}\cdot[A^{n-}_{x/n}\cdot mH_2O]^{x-}$, where M^{2+}=Zn, Cu, Ni, M^{3+}=Al, x = 0.33, n = 2 and A = CO_3^{2-}, were studied by X-ray diffraction, Fourier transform infrared spectroscopy, scanning electron microscopy and thermogravimetric analysis coupled with mass spectrometry (TG-MS). Different thermal behaviors upon heating were observed depending on the LDH composition, resulting in the exploitation of different calcination temperatures to convert LDH into mixed metal oxides (MMO). MMO were exposed to ambient air or pure carbon dioxide atmosphere to evaluate CO_2 adsorption properties. Aging in ambient condition leads to adsorption of both CO_2 and water, from ambient moisture, with variable ratios depending on the MMO composition. Furthermore, all the MMO were demonstrated to be able to adsorb CO_2 in pure gas stream, in the absence of moisture. In both ambient and pure CO_2 conditions, the performance of MMO is strongly dependent on the metal composition of MMO. In particular, the presence of Cu in the structure turned out to be beneficial in terms of adsorption capacity, with a maximum mass gain for CuAl MMO of 4 and 15% in pure CO_2 and in atmospheric conditions, respectively.

Keywords LDH · MMO · CO_2 adsorption · Chemisorption · Physisorption

Introduction

Different materials can be exploited for the CO_2 adsorption [1], including zeolites [2, 3], silicoaluminophosphates [4], activated carbons [5–8], metal-organic frameworks [9], porous polymers and amines, typically supported over mesoporous inorganic materials [10]. Layered double hydroxides (LDH) [11], also known as hydrotalcite-like compounds or anionic clays, appear to be very interesting as precursors for the preparation of CO_2 adsorbers, owing to both chemical structure and high surface area. LDH consist of positively charged brucite-like layers balanced by exchangeable anions in the interlayer. LDH have the general formula:

$$M^{2+}_{1-x}M^{3+}_{x}(OH)_2\cdot(CO_3)_{x/2}\cdot mH_2O \quad (1)$$

where M^{3+} (Al, Fe, Cr, Ga) partially substitutes M^{2+} (Ni, Mg, Zn, Cu, etc.) in the octahedral positions of the brucite-like hydroxides layers. A^{n-} is the interlayer anion (CO_3^{2-}, NO^{3-}, SO_4^{2-}, Cl^-, OH^-, etc.). The value of x [$x = M^{3+}/(M^{3+}+M^{2+})$] normally ranges between 0.17 and 0.33 [11–15]. It is worth noting that LDH composition can be finely tuned, and ternary LDH (where M^{2+}_{1-x} is a combination of two bivalent metals) can be synthetized [16–20].

Electronic supplementary material The online version of this article (https://doi.org/10.1007/s10973-018-7152-8) contains supplementary material, which is available to authorized users.

✉ A. Fina
alberto.fina@polito.it

[1] Politecnico di Torino, Sede di Alessandria, Viale Teresa Michel 5, 15121 Alessandria, Italy

[2] Prolabin & Tefarm S.r.l., Via dell'Acciaio 9, Ponte Felcino, 06134 Perugia, Italy

Thermal decomposition of these clays, particularly that of carbonate-exchanged LDH, was described to occur in three steps [21–23]: (1) release of the interlayer and the adsorbed water to obtain a metastable structure, (2) dehydroxylation of the brucite-like layers and (3) decomposition of the carbonates leading to the formation of metal mixed oxides (MMO). However, other authors divide the thermal decomposition of LDH in two stages: In the first one, at temperatures lower than 200 °C, the interlayer and the physisorbed water are lost, while in the second stage both CO_2 and structural water are simultaneously eliminated [24–26]. The dehydration and decarbonation of a LDH result in the formation of MMO:

$$M^{2+}_{1-x}M^{3+}_{x}(OH)_2 \cdot (CO_3)_{x/2} \cdot mH_2O \rightarrow MMO + CO_2 + H_2O \quad (2)$$

Even though there is no doubt that MMO heated at relatively low temperatures retain a structural homogeneity, the local ordering mechanism is not well understood. In a review, Forano et al. [11] proposed some different models for local ordering or segregation in the calcined LDH: One implicates the formation of layered double oxides [6] that can be intercalated by anions, whereas another model involves the formation of a pre-spinel phase. However, several studies report that at lower calcination temperatures, the segregation of oxidized phases including tenorite (CuO), cuprite (Cu_2O), periclase (MgO), zincite (ZnO), maghemite (γ-Fe_2O_3), etc., depending on the composition of the starting LDH [27, 28], is expected. Furthermore, when the calcination temperature is further increased, the diffusion of the trivalent metal into the bivalent oxides leads to the formation of spinels, i.e., to the loss of layered structure. The use of MMO as carbon dioxide adsorbers at high temperatures is widely discussed in the literature, mainly as gas separator from industrial fuel gases in power plants [29–33]. For instance, Wang et al. [34] showed good performances of these materials in the temperature range between 200 and 400 °C. The CO_2 adsorption efficiency depends on a wide number of variables, including the calcination temperature [23, 29], the interlayer anions [30], the type of trivalent metal ions [35] and the aluminum content [32]. Reddy et al. [29] as well as Hutson and Attwood [30] showed that two different mechanisms of adsorption are possible: reversible physisorption, which generally gives the higher contribution, and irreversible chemisorption. A few papers deal with the adsorption kinetic of MMO, with consistent results: The adsorption saturation typically occurs in few hours; however, in less than 10 min the 60–70% of the overall CO_2 adsorption capability is usually reached [23, 33, 35].

In this study, the CO_2 adsorption properties of MMO obtained from LDH containing different bivalent metals (Zn, Cu, Ni) are studied at ambient temperature and pressure, aiming at applications for CO_2 scavenging at room temperature. Adsorption and desorption were evaluated by a simple gravimetric method using TGA in variable temperature and gas.

Experimental

Synthesis and characterization of LDH and MMO

Four different kinds of LDH were synthesized in carbonate form, containing one bivalent and one trivalent metal ion (binary LDH) or two bivalent and one trivalent metal ion (ternary LDH) in the brucite-like layers.

LDH containing Zn and Al (labeled as ZnAl), Zn, Cu and Al (labeled as ZnCuAl), and Ni and Al (labeled as NiAl) were synthesized by the urea method [36]. Briefly, 0.5 M aqueous solutions of $Al(NO_3)_3{\cdot}9H_2O$ and $Zn(NO_3)_2{\cdot}6H_2O$ (for the synthesis of ZnAl), $Al(NO_3)_3{\cdot}9H_2O$, $Zn(NO_3)_2{\cdot}6H_2O$ and $Cu(NO_3)_2{\cdot}3H_2O$ (for the synthesis of ZnCuAl), or $Al(NO_3)_3{\cdot}9H_2O$ and $Ni(NO_3)_2{\cdot}6H_2O$ (for the synthesis of NiAl) in the proper volume ratio were added to solid urea, in molar ratio 10 versus Al, and then refluxed for 3 days. Finally, LDH were separated from the mother solution by centrifugation. Precipitates were then washed twice with deionized water and dried in oven at 80 °C.

LDH containing Cu and Al (CuAl) were synthesized by the co-precipitation method. Solutions 0.5 M of $Al(NO_3)_3{\cdot}9H_2O$ and $Cu(NO_3)_2{\cdot}3H_2O$ were mixed in the proper volume ratio; a NaOH solution 1 M was added at room temperature under stirring until pH = 8 was reached. At this point, LDH were separated from the solution by centrifugation. Precipitates were washed twice with deionized water and dried in oven at 80 °C.

Metals content in the different LDH was determined by inductively coupled plasma optical emission spectrometer (ICP-OES) Varian 700-ES, after dissolving the samples in concentrated HNO_3 and properly diluting them.

X-ray diffraction (XRD) analyses were performed at room temperature using a X'Pert (Philips, NL) X-ray diffractometer ($\lambda(CuK_\alpha)$ = 1.540562 Å) in configuration θ/θ on powders. XRD data were recorded in the 5°–80° 2θ range with a scan rate of 1° min^{-1}. No filtering was carried out on XRD spectra, which are reported as obtained. The LDH's lattice parameters, a and c, were determined using the following formulas: $a = 2d_{110}$ and $c = (3d_{003} + 6d_{006})/2$ [37]. The mean coherence length, L, was calculated from the FWHM values of the (003), (006) and (110) diffraction lines using the Scherrer equation.

Fourier transformed infrared spectroscopy (FTIR) experiments were carried out by a Frontier FTIR spectrometer (PerkinElmer, USA). Nanoparticles were mixed with KBr (< 1 mass% of LDH in KBr) to prepare KBr pellets. Spectra were collected in transmission mode at room temperature in the range 4000–400 cm^{-1} (16 scans and 4 cm^{-1} resolution).

The morphology of the samples was investigated with a FEG LEO 1525 field-emission scanning electron microscope (FE-SEM). FE-SEM micrographs were collected after depositing the samples on a stub and sputtering a chromium coating for 20 s.

Calcination

The calcination temperatures were selected based on the temperature measured in TGA (PerkinElmer Pyris 1, 10 °C min^{-1}, air stream, 10 ± 0.5 mg, platinum crucibles) for complete elimination of structural water upon heating. Once the temperature was selected, isothermal calcination treatments were carried out in a muffle for 90 min in air, using Al_2O_3 crucibles. The calcined LDH were then took out from the oven, fast cooled to room temperature and put into an hermetically closed vial under nitrogen (N_2) to prevent undesired CO_2 adsorption.

The as-obtained MMO are identified as ZnAlO, ZnCuAlO, CuAlO and NiAlO, depending on the starting LDH.

CO_2 adsorption measurement

Two different experimental methods were exploited to evaluate the CO_2 adsorption capability of MMO:

1. After calcination in the muffle, MMO were exposed for 7 days in ambient air conditions (23 °C, 50% RH). Then, CO_2 desorption was studied by heating samples (10 ± 0.5 mg) in a thermogravimetric analyzer (TGA) (TGA/SDTA851e, Mettler-Toledo, CH) from 25 °C up to the calcination temperature, at 10 °C min^{-1}, argon flux (50 mL min^{-1}), Al_2O_3 crucible. The amount of adsorbed CO_2 was indirectly calculated by the difference between gases evolved on heating after/before exposure. TGA was equipped with a mass spectrometer (ThermoStarGSD 300 T3 mass spectrometer, Pfeiffer Vacuum, D) to characterize gases released by MMO;
2. LDH were directly calcined in a TGA (TGA Q500, TA Instrument, USA) followed by immediate exposure of the as-obtained MMO to pure CO_2 flux in the TGA to measure online the mass increase associated with the CO_2 adsorption. The complete procedure is reported as follows:
   - LDH (about 10 mg) were calcined for 90 min at the selected temperature under nitrogen flux (60 mL min^{-1}), obtaining MMO;
   - After calcination, the furnace was cooled at 35 °C in nitrogen;
   - Then, the gas flux was switched to pure carbon dioxide (60 mL min^{-1}) for 120 min at 35 °C[1];
   - The gas was switched again to nitrogen (60 mL min^{-1}) and the desorption was carried out for 120 min at 35 °C;
   - Finally, a temperature ramp from 35 to 800 °C at a heating rate of 10 °C min^{-1}, under nitrogen flux (60 mL min^{-1}), was used to analyze the amount of chemisorbed CO_2.

Results and discussion

LDH characterization

The CO_2 adsorption properties of MMO are directly related to their composition and structure that depend on the characteristics of pristine LDH, as well as on the calcination temperature. For this reason, in this first section a thorough characterization of LDH will be carried out. The cation composition of the as-prepared LDH was determined by means of ICP-OES measurement on samples dissolved in nitric acid. The results are reported in Table 1 and show that the measured molar ratios of cations are close to the designed amount of metals. X-ray diffraction patterns of pristine LDH are reported in Fig. 1, whereas the LDH lattice parameters, a and c, and the mean coherence length, L, calculated from XRD analysis are reported in Table 1. ZnAl, ZnCuAl and CuAl spectra show the typical profile of hydrotalcite-like materials intercalated with carbonate anions [38], indicated by the presence of 003 and 006 planes reflection located at $2\theta = 11.63°$ (∼ 7.61 Å) and 23.25°, respectively. Furthermore, these three LDH exhibit comparable a and c parameters, which can be explained by the similar atomic radius of the bivalent cations (73 and 72 pm for Cu^{2+} and Zn^{2+}, respectively [39]). Instead, the reflection for the (003) planes of NiAl is located at $2\theta \approx 10.95°$, i.e., about 8.08 Å, with the a and c parameters equal to 0.307 and 2.415 nm, respectively. While the value of the a parameter is close to those measured for the other LDH, explained by the ionic radius of Ni^{2+} (69 pm [39]) close to those of Cu^{2+} and Zn^{2+}, the higher c parameter reflects the higher interlayer distance, owing to the presence of nitrates in the interlayer region [38], caused by an incomplete ion exchange (from nitrate

[1] This temperature was selected as the lowest possible temperature for the instrument and is sufficiently close to the ambient temperature.

Table 1 Cation composition, lattice parameters, *a* and *c*, and mean coherence length, *L*, of the as-prepared LDH

LDH	Cation content/mol%				Lattice parameters		
	Zn	Cu	Ni	Al	*a*/nm	*c*/nm	*L*/nm
ZnAl	67	–	–	33	0.307	2.280	28.0
ZnCuAl	8	60	–	32	0.307	2.282	24.1
CuAl	–	67	–	33	0.305	2.271	24.9
NiAl	–	–	67	33	0.307	2.415	10.7

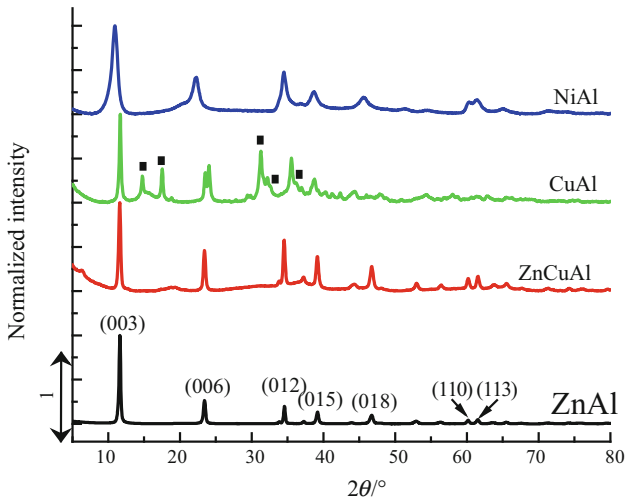

Fig. 1 XRD patterns for ZnAl, ZnCuAl, CuAl and NiAl pristine LDH. The symbol (square) indicates malachite reflections

to carbonate) during NiAl LDH synthesis. However, NiAl LDH containing carbonate ions were reported in the literature also with an interlayer distance ranging between 7.9 and 8.0 Å [36, 40], hence close to the value measured in the present paper. ZnAl, ZnCuAl and NiAl are constituted by pure hydrotalcite phase, whereas the XRD patterns of CuAl LDH contain several extra peaks, evidencing the presence of malachite (Fig. 1), a copper hydroxide carbonate [41–43]. The lower stability of the copper-containing hydrotalcite phase and the subsequent formation of malachite can be explained by the Jahn–Teller effect in the Cu^{2+} ion [44]. Therefore, in the ternary ZnCuAl LDH the copper concentration was kept below the limit of 25% of the total metal mole content to avoid the formation of malachite, as previously reported by Costantino et al. [18]. The mean coherence length, *L*, which is related to the structure ordering, was evaluated from broadening of LDH (003), (006) and (110) diffraction lines using the Scherrer equation. ZnAl, CuAl and ZnCuAl LDH exhibit *L* values in the range 24–28 nm, with the highest value for ZnAl, whereas the calculated L for NiAl is 10.7 nm.

The FTIR spectra (Fig. S1) of LDH provide information about the anion type in the interlayer region. In particular, two peaks appear in the nitrate/carbonate region (1350–1400 cm^{-1}) for all the LDH, with the exception of CuAl, which exhibits only one peak centered at $\sim$ 1385 cm^{-1}. This peak is assigned to the ν_3 mode of CO_3^{2-} [38]. All the other LDH exhibit the presence of a second peak, centered at $\sim$ 1355 cm^{-1}. This peak is assigned to the ν_3 mode of NO_3^- [33], thus suggesting an incomplete nitrate/carbonate exchange during the synthesis of LDH. Indeed, the intensity of this peak is higher in NiAl, thus further proving a high content of nitrates in the interlayer region of this LDH. However, in the literature the location of the vibration peaks of carbonate and nitrate ions is highly controversial, as the ν_3 mode of NO_3^- and CO_3^{2-} was also reported to occur at $\sim$ 1380 and 1360 cm^{-1}, respectively [26, 45, 46].

The morphology of the synthesized LDH was investigated by FE-SEM (Supplementary Information, Fig. S2). ZnAl (Fig. S2a) and NiAl (Fig. S2d) exhibit flat- and hexagonal-shaped crystals, with a thickness of some tens of nanometers and lateral size within the range 500–5 μm. ZnCuAl (Fig. S2b) is formed by irregular lamellar structure and a particle size < 500 nm. CuAl (Fig. 2) is characterized by the presence of two kinds of crystals (in agreement with XRPD) related to the presence of LDH and Malachite phases.

Thermal decomposition of LDH

The study of the thermal decomposition was preliminarily carried out to select the temperatures required for the calcinations of the different LDH. Indeed, the calcination temperature is crucial to obtain a high specific surface area and sufficient basicity of the adsorbing sites on the surface. According to previously reported results [23, 29, 32], the calcination temperature should be high enough to dehydrate and decarbonate the structure to MMO while

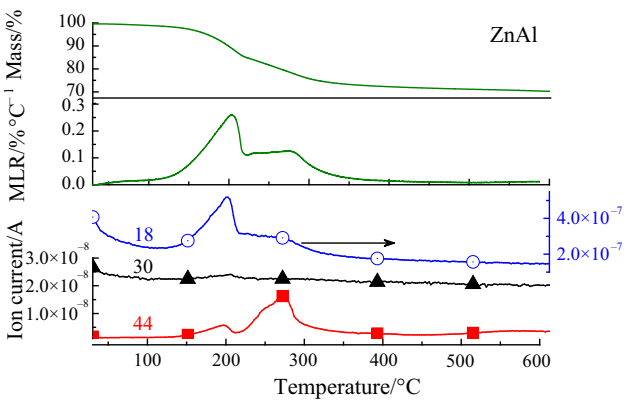

Fig. 2 ZnAl TGA mass, mass loss rate (MLR) and related MS plot

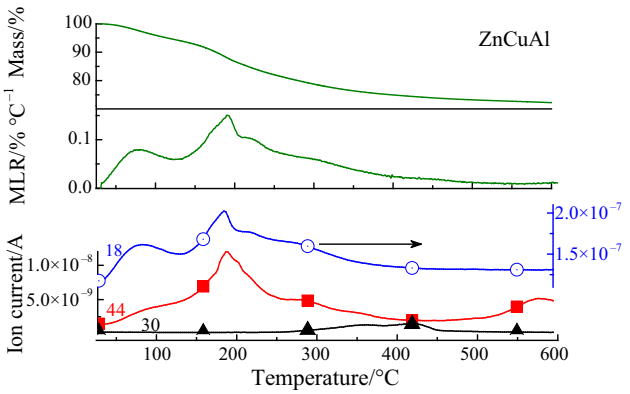

Fig. 3 ZnCuAl TGA mass, mass loss rate and related MS plot

avoiding the formation of spinel structure, which may be obtained at high temperature and which is not reversible to LDH [11].

The thermal decomposition was studied by TGA coupled with the mass spectrometer (TG-MS). TGA mass and mass loss rate (MLR) plots as well as selected MS plots for each material are reported in Figs. 2–5. MS plots of interest are m/z = 18 for H_2O, m/z = 30 for NO and m/z = 44 for CO_2; no other products were identified in the evolved gases by the analysis of the several other m/z signals.

ZnAl LDH (Fig. 2) showed the onset of thermal volatilization at about 150 °C, the mass loss at this temperature being about 2 mass%. Above 150 °C, water and CO_2 are simultaneously released in two partially overlapping steps. The first one is observed between 150 and 200 °C, probably related to the degradation of bidentate carbonates and the few remaining nitrate groups, whereas the second one occurs in the temperature range from 200 to 400 °C, assigned to monodentate carbonates [23]. At the end of these two steps the mass loss by ZnAl was about 27 mass%. Above 400 °C a progressive slow mass loss is observed to a total of 30 mass% at 600 °C, which is consistent with the theoretical mass loss for the conversion of ZnAl LDH to the oxide, i.e., about 33%. During this high-

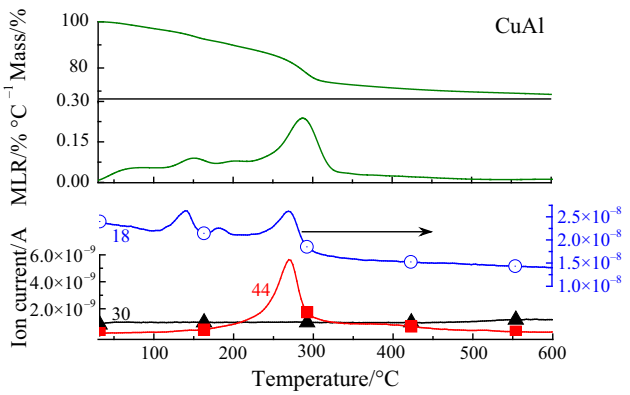

Fig. 4 CuAl TGA mass, mass loss rate (MLR) and related MS plot

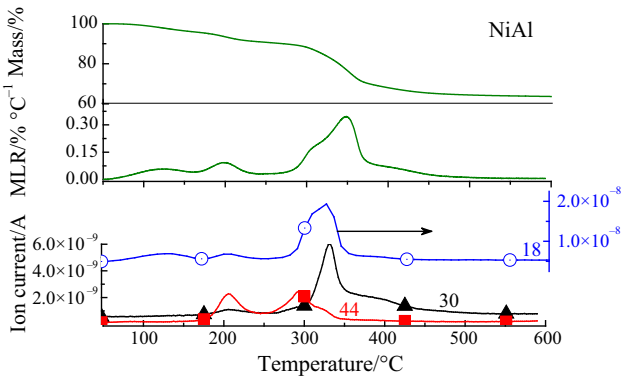

Fig. 5 NiAl TGA mass, mass loss rate (MLR) and related MS plot

temperature mass loss, CO_2 is continuously released over the entire temperature range, with no other associated products detectable.

Thermal volatilization of ZnCuAl is reported in Fig. 3: H_2O and CO_2 release starts at about 60 °C, whereas above 250 °C NO is released in traces, evidencing the presence of few residual nitrate groups from the synthesis of this LDH. Finally, above 500 °C a second minor CO_2 release is observed, which might be related to monodentate carbonate anions. The residue at 600 °C is about 72 mass%, which is slightly higher than the theoretical conversion to oxide (theoretical residue = 68%).

Thermal decomposition of CuAl (Fig. 4) can be divided into two main steps. The first mass loss, observed until 200 °C, corresponds to interlayer water loss coupled with initial development of CO_2. In the second step, between 200 and 400 °C, a further loss of about 20 mass% of the initial mass is observed, mainly due to the release of carbon dioxide. NO was not detected, and no other relevant products are released on heating, leading to a residue of about 68 mass% at 600 °C, which is consistent with the theoretical residue (about 67 mass%).

NiAl LDH (Fig. 5) shows a more complex decomposition pathway: In the first step (50–150 °C) weakly adsorbed water is mainly released; in the second step (150–250 °C) interlayer water and weakly bonded carbonate ions are volatilized; above 250 °C, the main dehydroxylation and decarbonation step occurs, partially overlapped with the release of NO, evidencing the coexistence of carbonate and nitrate LDH forms, accordingly with XRPD and FTIR analyses. At 600 °C the decomposition of NiAl LDH is completed with a residue of about 64 mass%, in good agreement with the theoretical value, i.e., 66 mass%.

Based on the TGA and MS evidences, the endset temperatures for the decarbonation/denitration were taken as the calcination temperatures, to be carried out in isothermal conditions. At the end of the isothermal treatments, residual weights obtained were quite consistent with theoretical

Table 2 Calcination temperatures for the different LDH

LDH	Calcination temperatures/°C	Residue at the end of isothermal treatment/%	Theoretical residue/%
ZnAl	350	71.3	67
ZnCuAl	400	70.5	68
CuAl	400	63.9	67
NiAl	450	63.2	66

predictions and residues obtained after heating in TGA (Table 2). Deviations in the final residue may be due to impurities in the LDH, either as a different balance between carbonate and nitrate forms or as minor inclusions of second phases, theoretical residue calculation being calculated on ideal carbonate LDH.

Characterization of MMO

MMO freshly obtained from calcination were characterized by XRPD and SEM, in order to evaluate crystalline and structure evolution during calcination, as well as by FTIR and TGA, to study gas adsorption during rapid cooling to room temperature at the end of thermal treatments.

XRD diffraction patterns for the different MMO (Fig. S3) show dramatic changes in the crystalline structure respect to pristine LDH (Fig. 1). Indeed, the reflections typical for brucite-like layers in LDH disappeared, whereas new peaks are observed, hence evidencing the formation of metal mixed oxide phases. This structural evolution can be expected, owing to the decarbonation/denitration and dehydroxylation occurring upon thermal heating of LDH, with the loss of the LDH structure at temperature close to 200 °C and the formation of different crystalline phases depending on the calcination temperature, as reported in the literature [12, 28, 37, 47–49]. In particular, comparing TG-MS data and XPRD data in the present work with in situ XRPD reported by Jabłońska et al. [28], for ZnAl and ZnCuAl systems, Alejandre et al. [49], for CuAl LDH, and Alejandre et al. [48], for NiAl systems, showed the complete loss of LDH order at temperatures higher than 150 °C, with the formation of mixed oxides including zincite (ZnO), tenorite (CuO) and bunsenite (NiO), whereas spinel phases are obtained at higher temperatures. Despite the evolution in the crystalline structure of MMO, no significant morphological alterations were observed after calcination of LDH, as SEM micrographs (Fig. S4) show similar morphologies between LDH and fresh MMO, with crystals agglomerates exhibiting lateral size in the range 200–2 μm and thicknesses of few tens of nanometers. FTIR analysis (Fig. S5) evidences the almost complete release of water molecules. Indeed, the broad adsorption band at 3400–3500 cm^{-1}, corresponding to the ν_{OH} vibration, and the peak at ~ 1640 cm^{-1}, related to the δ_{HOH} of water molecules, disappear after calcination of the different LDH. Furthermore, no clear signals owing to the presence of carbonate or nitrate anions are visible in ZnAl, ZnCuAl and NiAl, whereas the presence of a peak centered at ~ 1385 cm^{-1} (ν_3 mode of CO_3^{2-}) in CuAl indicates for an incomplete decarbonation. The presence of carbonates after calcination was observed also in the literature for ZnAl LDH and related to the partial persistence of the layered structure [50]. On the other hand, the release of CO_2 upon thermal decomposition of malachite was reported to occur at temperatures lower than the calcination temperature exploited in the present paper for CuAl LDH [51, 52]. Finally, thermogravimetric analysis (10 °C min^{-1}, up to the calcination temperature, nitrogen atmosphere) performed on fresh MMO (Fig. S6) reveal about 2–5 mass% mass loss at temperature below 200 °C for all the oxides, evidencing the physisorption of limited amount of gases from the atmosphere.

CO_2 adsorption/desorption of MMO

Ambient atmosphere exposure

Calcined LDH were aged for 7 days in ambient atmosphere to allow CO_2 adsorption. After exposure, the mass loss by MMO was evaluated by TGA by a temperature ramp up to the calcination temperature, to determine the amount of desorbed CO_2 and moisture. As the calculation of relative amounts of water and CO_2 adsorbed is not trivial, the two products being released simultaneously, TGA coupled with mass spectroscopy was used to detect the presence of CO_2 in the desorbed gas from atmosphere-exposed MMO. Results from thermogravimetry and MS plots for water (m/z = 18) and CO_2 (m/z = 44) are reported in Figs. 6–9 for aged ZnAlO, ZnCuAlO, CuAlO and NiAlO, respectively. TGA plots of aged and fresh MMO are compared to quantify the amount adsorbed CO_2 and moisture during the

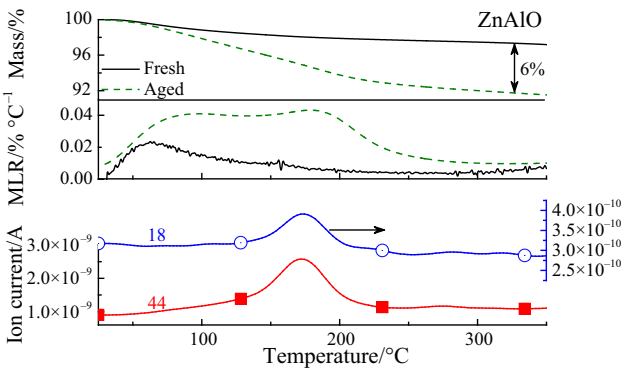

Fig. 6 ZnAlO TGA mass, mass loss rate (MLR) and related MS plot

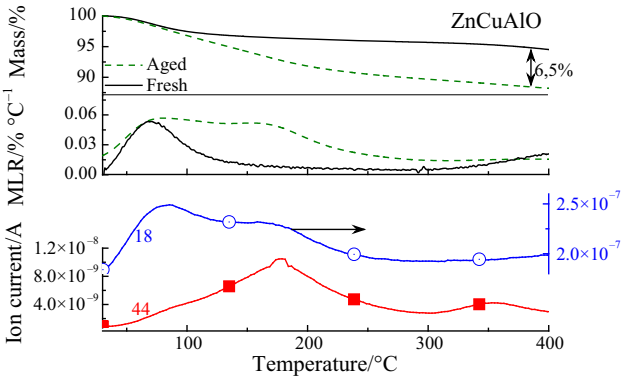

Fig. 7 ZnCuAlO TGA mass, mass loss rate (MLR) and related MS plot

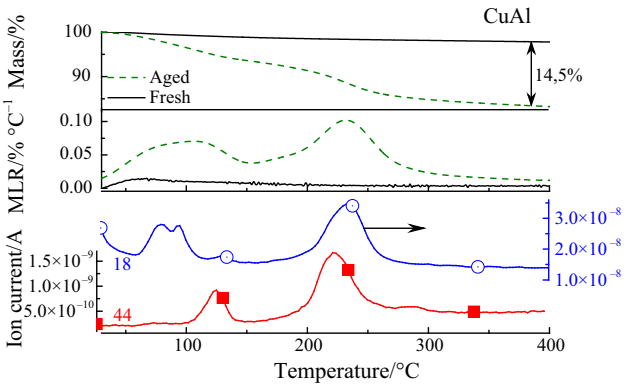

Fig. 8 CuAlO TGA mass, mass loss rate (MLR) and related MS plot

ambient exposure. For all the MMO studied, XRPD after ambient exposure revealed no significant differences between the fresh and ambient-aged MMO (Fig. S7), evidencing no reconstruction of the initial LDH structure.

Both fresh and aged ZnAlO (Fig. 6) exhibit a mass loss starting at about 50 °C and completed at 250 °C, corresponding to about 2 and 8 mass% loss, respectively. However, for fresh LDO only one broad peak with maximum mass loss rate at about 63 °C is observed, evidencing only one mass loss step, whereas in aged ZnAlO two clear peaks (at about 92 and 180 °C) are observed in the MLR plot, suggesting for two different stages in mass loss. Indeed, simultaneous release of CO_2 and water is proven in aged ZnAlO, evidencing their adsorption from the ambient atmosphere during exposure. It is worth noting that total mass loss on heating for the aged ZnAl MMO is much lower than the one observed in the same temperature range for the pristine ZnAl LDH (Fig. 2), confirming that the adsorption of CO_2 and moisture does not lead to the reconstruction of LDH structure, at least in the exposure conditions used in this work.

Aged ZnCuAlO (Fig. 7) releases about 12 mass% of the initial mass upon heating to 400 °C, which is assigned by MS signals to carbon dioxide and water vapor, which are released in two partially overlapped steps in the temperature range up to the calcination temperature used. Comparing ZnCuAlO with ZnAlO, differences are observed in the total mass loss on heating, reflecting moisture and CO_2 adsorption. Therefore, the partial substitution of Zn by Cu was proven to affect the adsorption properties of LDH, especially for moisture, as suggested by the water plot in the MS plot for aged ZnCuAlO.

During desorption on heating from aged CuAlO (Fig. 8), three release steps are distinguishable in both MLR and MS curves: The first in the temperature range of about 50–120 °C is mainly related to the loss of water (about 5 mass%), immediately followed by an overlapped mass loss peak related to the release of CO_2. The third mass loss step occurs in the broad temperature range between 150 and 300 °C and corresponds to the simultaneous release of water and carbon dioxide (about 7 mass%). The overall mass released was measured as about 15 mass%, CuAlO therefore being more efficient in adsorbing water and CO_2 as compared to ZnAlO and ZnCuAlO in ambient atmosphere, which is likely related to the modifications induced by copper into the MMO structure.

Fresh and aged NiAlO (Fig. 9) release about 3 and 5.5 mass%, respectively, during TGA up to the calcination temperature, the difference between fresh and aged MMO suggesting a limited sorption capability in ambient conditions. Furthermore, the mass loss plot for aged NiAlO is quite different from those of the MMO previously discussed. Indeed, for NiAlO a single very broad mass loss step is observable, resulting in a slow and progressive mass loss caused by CO_2 releases in the temperature range 50–250 °C, whereas the amount of moisture released is negligible.

Based on the results presented in this section, the most effective adsorber in ambient conditions was CuAlO, followed by ZnCuAlO, confirming the importance of Cu cations for the increase in sorption efficiency. The higher adsorption properties of CuAlO and ZnCuAlO can be

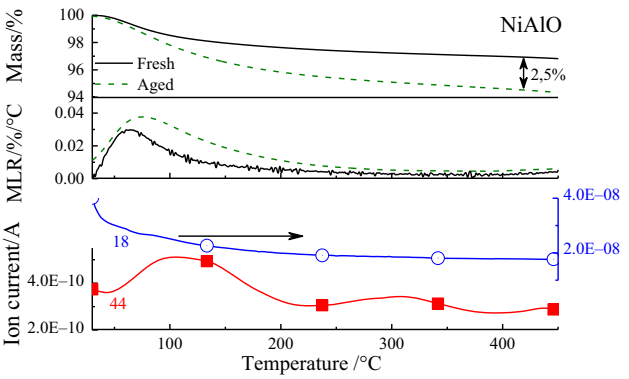

Fig. 9 NiAlO TGA mass, mass loss rate (MLR) and related MS plot

related to the effect of Cu^{2+} on the basicity, which allows for CO_2 adsorption [53], of the MMO or on the morphology of the pristine and calcined LDH. Indeed, Kovanda et al. [27] showed an increase in the basic sites per square meter for CuAlO with respect to MgAlO, which can explain the higher CO_2 adsorption capacity of CuAlO. However, the morphology of copper-containing MMO might also play a role, as these two materials exhibit a similar morphology, with the presence of a large amount of small particles, whereas ZnAlO and NiAlO are made of larger nanoparticles.

Carbon dioxide flux exposure

To further investigate the CO_2 adsorption dynamic, treatments in pure CO_2 atmosphere were carried out in thermogravimetry close to the ambient temperature.

An integrated procedure was used,[2] including calcination, CO_2 adsorption in isothermal conditions (35 °C), desorption in nitrogen in isothermal conditions (35 °C) and final heating for complete desorption in temperature ramp. Isothermal adsorption, isothermal desorption and heating ramp desorption results are reported in Fig. 10, separately for each step. In the graphs, initial mass at the beginning of each step was normalized to 100% for the sake of comparison.

In Fig. 10a, isothermal adsorption for the different MMO are presented. Different mass versus time plots were obtained for the different MMO; a two-step mass increase was found for all the products, with a first relatively fast in a few initial minutes, followed by a slower and progressive mass gain in time. Furthermore, for all the MMO, except CuAlO, the rate of mass increase in the second step was found to be approximately constant. The extent of total adsorbed CO_2 after the 120-min treatment was found to be very different for the different MMO, being about 4% for CuAlO, 3% for ZnCuAlO, 2% for NiAlO and 1% for ZnAlO.

This trend is not completely consistent with the MMO ranking in adsorption efficiency in ambient conditions described above. CuAlO and ZnCuAlO are confirmed as the most efficient adsorbers, whereas NiAlO and ZnAlO showed different performances in ambient and pure CO_2 conditions. Indeed, while NiAlO seems to be able to adsorb CO_2 independently on moisture, ZnAlO seems to be more effective in ambient conditions, where moisture is available. This may suggest a different role of water in fixing CO_2 on the different LDH structures, which is still not clear and will require further research efforts.

[2] For the detailed description of the method, see Experimental section.

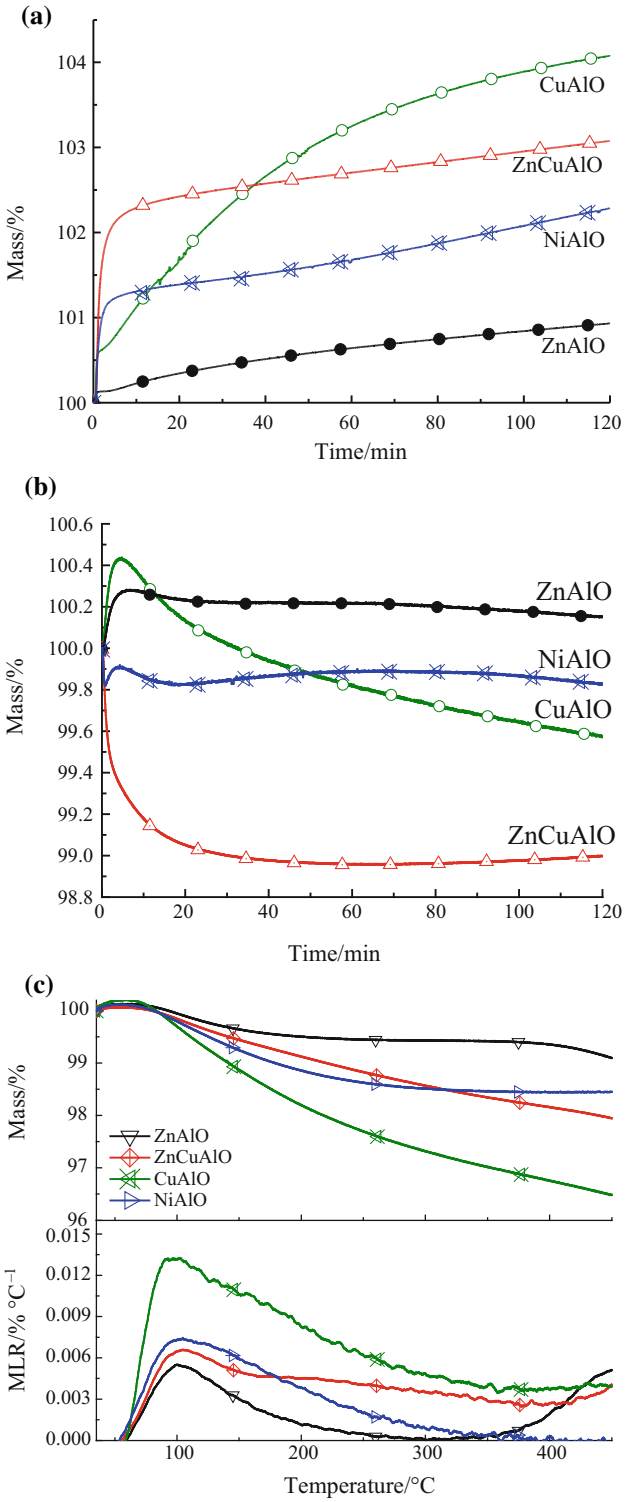

Fig. 10 CO_2 **a** isothermal adsorption, **b** physisorbed desorption and **c** chemisorbed desorption

To evaluate the strength of CO_2 adsorption to the MMO structures, two steps of desorption were studied. In Fig. 10b, desorption in isothermal conditions (35 °C) with nitrogen flow is reported, showing negligible mass changes

for ZnAlO and NiAlO, whereas CuAlO and ZnCuAlO were found to release about 0.8 and 1 mass%, respectively. The mass lost by MMO during this desorption step is assigned to weakly bound, physisorbed carbon dioxide. Therefore, we can assume that most of the CO_2 adsorbed by the MMO during the adsorption step is chemisorbed. In the heating ramp desorption step (Fig. 10c), thermal desorption peak occurs at about 100 °C for all the MMO, but the desorption extent varies for the different LDO, reflecting the extent of CO_2 adsorbed; indeed, the mass loss by MMO during heating is equivalent to the difference between the adsorbed and the desorbed in isothermal.

Conclusions

In this paper, the effect of bivalent metal cations (M^{2+}=Zn, Cu, Ni) on the CO_2 adsorption properties of metal mixed oxide (MMO), obtained upon calcination of LDH, was addressed. The formulations were obtained as well-crystallized LDH structures with the exception of CuAl LDH, where segregation of malachite was observed in addition to the expected LDH, explained by the Jahn–Teller effect in the Cu^{2+} cations. Besides the study of gases evolution, thermogravimetry showed differences in the temperature required for the complete release of water and CO_2 to obtain MMO. Values ranging between 350 and 450 °C were measured and selected aiming at the production of oxides able to capture CO_2 at room temperature.

After calcination, the sorption of CO_2 for different calcined MMO systems was indirectly evaluated by thermal desorption after exposure of MMO in ambient atmosphere or in pure CO_2, by the use of a simple and versatile thermogravimetric method.

When exposed to ambient atmosphere the MMO were shown to adsorb both carbon dioxide and water. However, depending on the metal substitution the ratio between CO_2 and H_2O adsorption is rather variable. In particular, NiAlO seems almost insensitive to moisture adsorption, whereas all other MMO displayed significant moisture adsorbance. Indeed, depending on the chemical structure, water can exhibit different tendencies to coordinate the carbon dioxide.

To decouple water and carbon dioxide adsorption on MMO, oxides were also exposed to pure CO_2 stream, which further confirmed strong differences in the adsorption amount and rate as a function of the type of bivalent metal. In particular, the presence of copper in the structure appears crucial to obtain high adsorption rates (4 mass% mass gain after 120-min exposure to CO_2 at 35 °C for CuAl, the best adsorbent in this study), which appear to be related to the distortion of the LDH structure (owing to the Jahn–Teller effect) or to the effect of copper cations on the basicity of adsorption sites.

Acknowledgements This research work was funded by "ITACA" project of the POR-FESR "Competitività regionale e occupazione" 2007/2013, Asse 1, Misura I.1.1, "Piattaforme innovative" of the Piedmont Region (Italy). Prof. Matteo Pavese at Politecnico di Torino is acknowledged for providing access to TG-MS equipment. Authors gratefully acknowledge A. Petracci and R. Spogli at Prolabin & Tefarm S.r.l for SEM analysis and the useful discussions. Furthermore, Prof. Giovanni Camino at Politecnico di Torino is gratefully acknowledged for discussion and interpretation of results.

References

1. Leung DY, Caramanna G, Maroto-Valer MM. An overview of current status of carbon dioxide capture and storage technologies. Renew Sustain Energy Rev. 2014;39:426–43.
2. Silva JA, Schumann K, Rodrigues AE. Sorption and kinetics of CO_2 and CH_4 in binderless beads of 13X zeolite. Microporous Mesoporous Mater. 2012;158:219–28.
3. Wang L, Liu Z, Li P, Yu J, Rodrigues AE. Experimental and modeling investigation on post-combustion carbon dioxide capture using zeolite 13X-APG by hybrid VTSA process. Chem Eng J. 2012;197:151–61.
4. Cheung O, Liu Q, Bacsik Z, Hedin N. Silicoaluminophosphates as CO_2 sorbents. Microporous Mesoporous Mater. 2012;156:90–6.
5. Yang R, Liu G, Li M, Zhang J, Hao X. Preparation and N_2, CO_2 and H_2 adsorption of super activated carbon derived from biomass source hemp (*Cannabis sativa* L.) stem. Microporous Mesoporous Mater. 2012;158:108–16.
6. Vargas DP, Giraldo L, Moreno-Piraján JC. CO2 adsorption on activated carbon honeycomb-monoliths: a comparison of Langmuir and Toth models. Int J Mol Sci. 2012;13(7):8388–97.
7. Correia LB, Fiuza RA, de Andrade RC, Andrade HM. CO_2 capture on activated carbons derived from mango fruit (*Mangifera indica* L.) seed shells. J Therm Anal Calorim. 2017;131:1–8.
8. Giraldo L, Moreno-Piraján JC. CO_2 adsorption on activated carbon prepared from mangosteen peel. J Therm Anal Calorim. 2017. https://doi.org/10.1007/s10973-017-6725-2.
9. Yu J, Xie L-H, Li J-R, Ma Y, Seminario JM, Balbuena PB. CO_2 capture and separations using MOFs: computational and experimental studies. Chem Rev. 2017;117(14):9674–754.
10. Qi G, Fu L, Choi BH, Giannelis EP. Efficient CO_2 sorbents based on silica foam with ultra-large mesopores. Energy Environ Sci. 2012;5(6):7368–75.
11. Forano C, Hibino T, Leroux F, Taviot-Gueho C. 1 layered double hydroxides. Dev Clay Sci. 2006;1:1021–95.
12. Hibino T, Yamashita Y, Kosuge K, Tsunashima A. Decarbonation behavior of Mg–Al–CO_3 hydrotalcite-like compounds during heat treatment. Clays Clay Miner. 1995;43(4):427–32.
13. Kloprogge JT, Frost RL. Fourier transform infrared and Raman spectroscopic study of the local structure of Mg-, Ni-, and Co-hydrotalcites. J Solid State Chem. 1999;146(2):506–15.
14. Stanimirova T, Kirov G. Cation composition during recrystallization of layered double hydroxides from mixed (Mg, Al) oxides. Appl Clay Sci. 2003;22(6):295–301.
15. Hutson ND, Speakman SA, Payzant EA. Structural effects on the high temperature adsorption of CO_2 on a synthetic hydrotalcite. Chem Mater. 2004;16(21):4135–43.

16. Kloprogge JT, Hickey L, Frost RL. FT-Raman and FT-IR spectroscopic study of synthetic Mg/Zn/Al-hydrotalcites. J Raman Spectrosc. 2004;35(11):967–74.
17. Porta P, Morpurgo S. Cu/Zn/Co/Al/Cr-containing hydrotalcite-type anionic clays. Appl Clay Sci. 1995;10(1–2):31–44.
18. Costantino U, Marmottini F, Sisani M, Montanari T, Ramis G, Busca G, et al. Cu–Zn–Al hydrotalcites as precursors of catalysts for the production of hydrogen from methanol. Solid State Ion. 2005;176(39):2917–22.
19. Valente JS, Hernandez-Cortez J, Cantu MS, Ferrat G, López-Salinas E. Calcined layered double hydroxides Mg–Me–Al (Me: Cu, Fe, Ni, Zn) as bifunctional catalysts. Catal Today. 2010;150(3):340–5.
20. Di Fronzo A, Pirola C, Comazzi A, Galli F, Bianchi C, Di Michele A, et al. Co-based hydrotalcites as new catalysts for the Fischer–Tropsch synthesis process. Fuel. 2014;119:62–9.
21. Węgrzyn A, Rafalska-Łasocha A, Majda D, Dziembaj R, Papp H. The influence of mixed anionic composition of Mg–Al hydrotalcites on the thermal decomposition mechanism based on in situ study. J Therm Anal Calorim. 2009;99(2):443–57.
22. Tao Q, He H, Frost RL, Yuan P, Zhu J. Thermal decomposition of silylated layered double hydroxides. J Therm Anal Calorim. 2010;101(1):153–9.
23. León M, Díaz E, Bennici S, Vega A, Ordónez S, Auroux A. Adsorption of CO_2 on hydrotalcite-derived mixed oxides: sorption mechanisms and consequences for adsorption irreversibility. Ind Eng Chem Res. 2010;49(8):3663–71.
24. Klemkaite K, Prosycevas I, Taraskevicius R, Khinsky A, Kareiva A. Synthesis and characterization of layered double hydroxides with different cations (Mg Co, Ni, Al), decomposition and reformation of mixed metal oxides to layered structures. Open Chem. 2011;9(2):275–82.
25. Othman M, Helwani Z, Fernando W. Synthetic hydrotalcites from different routes and their application as catalysts and gas adsorbents: a review. Appl Organomet Chem. 2009;23(9):335–46.
26. Gupta S, Agarwal DD, Banerjee S. Synthesis and characterization of hydrotalcites: Potential thermal stabilizers for PVC. Indian J Chem. 2008;47A:1004–8.
27. Kovanda F, Jirátová K, Rymeš J, Koloušek D. Characterization of activated Cu/Mg/Al hydrotalcites and their catalytic activity in toluene combustion. Appl Clay Sci. 2001;18(1):71–80.
28. Jabłońska M, Chmielarz L, Węgrzyn A, Guzik K, Piwowarska Z, Witkowski S, et al. Thermal transformations of Cu–Mg (Zn)–Al(Fe) hydrotalcite-like materials into metal oxide systems and their catalytic activity in selective oxidation of ammonia to dinitrogen. J Therm Anal Calorim. 2013;114(2):731–47.
29. Ram Reddy M, Xu Z, Lu G, Diniz da Costa J. Layered double hydroxides for CO_2 capture: structure evolution and regeneration. Ind Eng Chem Res. 2006;45(22):7504–9.
30. Hutson ND, Attwood BC. High temperature adsorption of CO_2 on various hydrotalcite-like compounds. Adsorption. 2008;14(6):781–9.
31. Ficicilar B, Dogu T. Breakthrough analysis for CO_2 removal by activated hydrotalcite and soda ash. Catal Today. 2006;115(1):274–8.
32. Yong Z, Mata V, Rodrigues AE. Adsorption of carbon dioxide onto hydrotalcite-like compounds (HTlcs) at high temperatures. Ind Eng Chem Res. 2001;40(1):204–9.
33. Zhu X, Shi Y, Cai N. High-pressure carbon dioxide adsorption kinetics of potassium-modified hydrotalcite at elevated temperature. Fuel. 2017;207:579–90.
34. Wang Q, Wu Z, Tay HH, Chen L, Liu Y, Chang J, et al. High temperature adsorption of CO_2 on Mg–Al hydrotalcite: effect of the charge compensating anions and the synthesis pH. Catal Today. 2011;164(1):198–203. https://doi.org/10.1016/j.cattod.2010.10.042.
35. Wang Q, Tay HH, Ng DJW, Chen L, Liu Y, Chang J, et al. The effect of trivalent cations on the performance of Mg–M–CO_3 layered double hydroxides for high-temperature CO_2 capture. Chemsuschem. 2010;3(8):965–73.
36. Costantino U, Marmottini F, Nocchetti M, Vivani R. New synthetic routes to hydrotalcite-like compounds-characterisation and properties of the obtained materials. Eur J Inorg Chem. 1998;1998(10):1439–46.
37. Basąg S, Kovanda F, Piwowarska Z, Kowalczyk A, Pamin K, Chmielarz L. Hydrotalcite-derived Co-containing mixed metal oxide catalysts for methanol incineration. J Therm Anal Calorim. 2017;129(3):1301–11.
38. Kloprogge JT, Wharton D, Hickey L, Frost RL. Infrared and Raman study of interlayer anions CO_{32-}, NO_{3-}, SO_{42-} and ClO_{4-} in Mg/Al-hydrotalcite. Am Miner. 2002;87(5–6):623–9.
39. Shannon RD. Revised effective ionic radii and systematic studies of interatomic distances in halides and chalcogenides. Acta Crystallogr Sect A Cryst Phys Diffr Theor Gen Crystallog. 1976;32(5):751–67.
40. Costantino U, Curini M, Montanari F, Nocchetti M, Rosati O. Hydrotalcite-like compounds as catalysts in liquid phase organic synthesis: I. Knoevenagel condensation promoted by $[Ni_{0.73}Al_{0.27}(OH)_2](CO_3)_{0.135}$. J Mol Catal A Chem. 2003;195(1):245–52.
41. Segal SR, Anderson KB, Carrado KA, Marshall CL. Low temperature steam reforming of methanol over layered double hydroxide-derived catalysts. Appl Catal A. 2002;231(1):215–26.
42. Lwin Y, Yarmo MA, Yaakob Z, Mohamad AB, Daud WRW. Synthesis and characterization of Cu–Al layered double hydroxides. Mater Res Bull. 2001;36(1):193–8.
43. Neves V, Costa M, Senra J, Aguiar L, Malta L. Thermal behavior of LDH 2CuAl. CO_3 and 2CuAl. CO_3/Pd. J Therm Anal Calorim. 2017;130(2):689–94.
44. Cavani F, Trifirò F, Vaccari A. Hydrotalcite-type anionic clays: preparation, properties and applications. Catal Today. 1991;11(2):173–301.
45. Resini C, Montanari T, Barattini L, Ramis G, Busca G, Presto S, et al. Hydrogen production by ethanol steam reforming over Ni catalysts derived from hydrotalcite-like precursors: catalyst characterization, catalytic activity and reaction path. Appl Catal A. 2009;355(1):83–93.
46. Goh K-H, Lim T-T, Dong Z. Application of layered double hydroxides for removal of oxyanions: a review. Water Res. 2008;42(6):1343–68.
47. Basąg S, Piwowarska Z, Kowalczyk A, Węgrzyn A, Baran R, Gil B, et al. Cu-Mg-Al hydrotalcite-like materials as precursors of effective catalysts for selective oxidation of ammonia to dinitrogen—the influence of Mg/Al ratio and calcination temperature. Appl Clay Sci. 2016;129:122–30.
48. Alejandre A, Medina F, Rodriguez X, Salagre P, Cesteros Y, Sueiras J. Cu/Ni/Al layered double hydroxides as precursors of catalysts for the wet air oxidation of phenol aqueous solutions. Appl Catal B. 2001;30(1):195–207.
49. Alejandre A, Medina F, Salagre P, Correig X, Sueiras J. Preparation and study of Cu–Al mixed oxides via hydrotalcite-like precursors. Chem Mater. 1999;11(4):939–48.
50. Seftel E, Popovici E, Mertens M, De Witte K, Van Tendeloo G, Cool P, et al. Zn–Al layered double hydroxides: synthesis, characterization and photocatalytic application. Microporous Mesoporous Mater. 2008;113(1):296–304.
51. Porta P, De Rossi S, Ferraris G, Jacono ML, Minelli G, Moretti G. Structural characterization of malachite-like coprecipitated precursors of binary CuO–ZnO catalysts. J Catal. 1988;109(2):367–77.
52. Behrens M, Girgsdies F, Trunschke A, Schlögl R. Minerals as model compounds for Cu/ZnO catalyst precursors: structural and thermal properties and IR spectra of mineral and synthetic

(zincian) malachite, rosasite and aurichalcite and a catalyst precursor mixture. Eur J Inorg Chem. 2009;2009(10):1347–57.
53. Smoláková L, Frolich K, Troppová I, Kutálek P, Kroft E, Čapek L. Determination of basic sites in Mg–Al mixed oxides by combination of TPD-CO_2 and CO_2 adsorption calorimetry. J Therm Anal Calorim. 2017;127(3):1921–9.